SANDIA REPORT

SAND2014-18207
Unlimited Release
Printed September 2014

Investigation of Spatial Variation of Sea States Offshore of Humboldt Bay, CA Using a Hindcast Model

Ann R. Dallman, Vincent S. Neary, Morgan Stephenson

Prepared by
Sandia National Laboratories
Albuquerque, New Mexico 87185 and Livermore, California 94550

Sandia National Laboratories is a multi-program laboratory managed and operated by Sandia Corporation, a wholly owned subsidiary of Lockheed Martin Corporation, for the U.S. Department of Energy's National Nuclear Security Administration under contract DE-AC04-94AL85000.

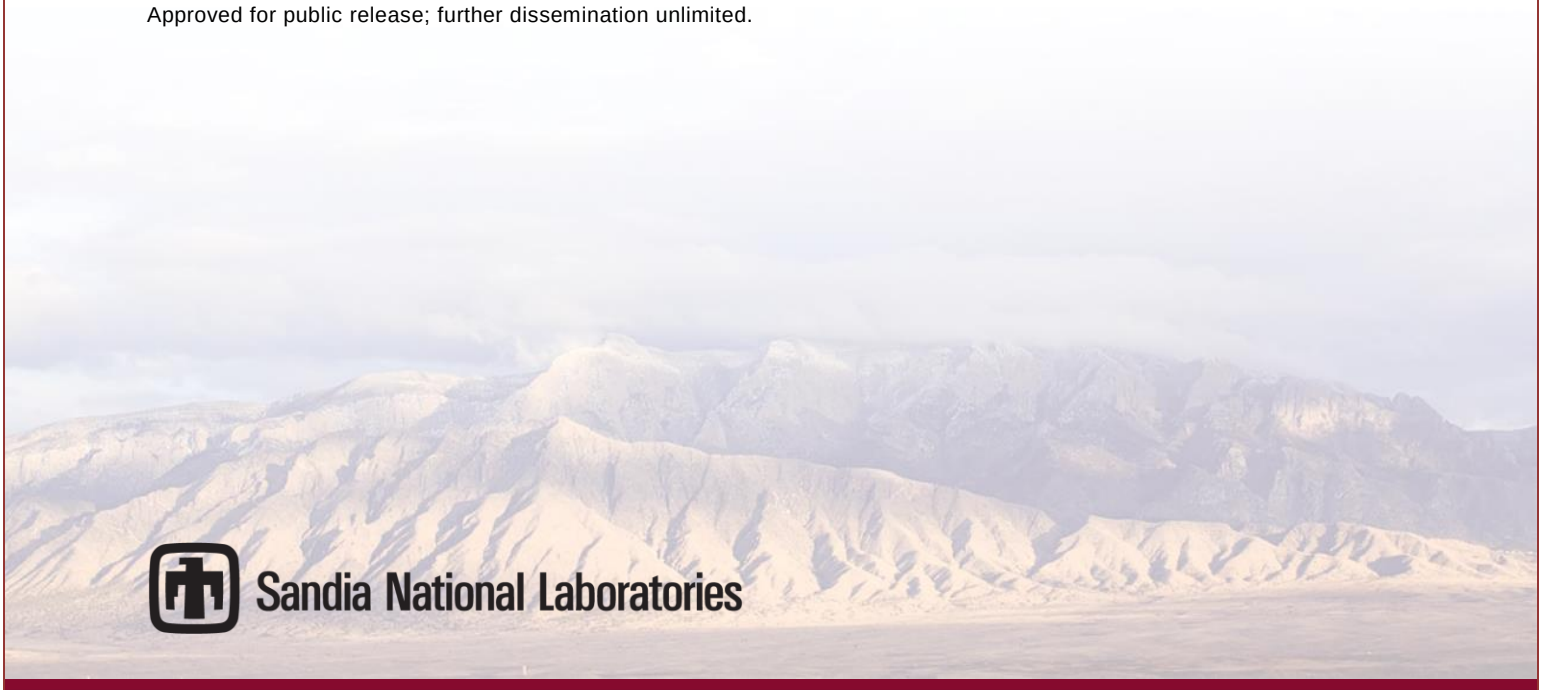

Sandia National Laboratories

Issued by Sandia National Laboratories, operated for the United States Department of Energy by Sandia Corporation.

Available to DOE and DOE contractors from
U.S. Department of Energy
Office of Scientific and Technical Information
P.O. Box 62
Oak Ridge, TN 37831

Telephone: (865) 576-8401
Facsimile: (865) 576-5728
E-Mail: reports@adonis.osti.gov
Online ordering: http://www.osti.gov/bridge

Available to the public from
U.S. Department of Commerce
National Technical Information Service
5285 Port Royal Rd.
Springfield, VA 22161

Telephone: (800) 553-6847
Facsimile: (703) 605-6900
E-Mail: orders@ntis.fedworld.gov
Online order: http://www.ntis.gov/help/ordermethods.asp?loc=7-4-0#online

SAND2014-18207
Unlimited Release
Printed September 2014

Investigation of Spatial Variation of Sea States Offshore of Humboldt Bay, CA Using a Hindcast Model

Ann R. Dallman, Vincent S. Neary
Water Power Technologies
Sandia National Laboratories
P.O. Box 5800
Albuquerque, New Mexico 87185-MS1124

Morgan Stephenson
Sea Engineering, Inc.
Makai Research Pier
41-305 Kalanianaole Hwy
Waimanalo, HI 96795

Abstract

Spatial variability of sea states is an important consideration when performing wave resource assessments and wave resource characterization studies for wave energy converter (WEC) test sites and commercial WEC deployments. This report examines the spatial variation of sea states offshore of Humboldt Bay, CA, using the wave model SWAN. The effect of depth and shoaling on bulk wave parameters is well resolved using the model SWAN with a 200 m grid. At this site, the degree of spatial variation of these bulk wave parameters, with shoaling generally perpendicular to the depth contours, is found to depend on the season. The variation in wave height, for example, was higher in the summer due to the wind and wave sheltering from the protruding land on the coastline north of the model domain. However, the spatial variation within an area of a potential Tier 1 WEC test site at 45 m depth and 1 square nautical mile is almost negligible; at most about 0.1 m in both winter and summer. The six wave characterization parameters recommended by the IEC 62600-101 TS were compared at several points along a line perpendicular to shore from the WEC test site. As expected, these parameters varied based on depth, but showed very similar seasonal trends.

ACKNOWLEDGMENTS

This study was supported by the Department of Energy (DOE), Office of Energy Efficiency and Renewable Energy (EERE), Wind and Water Power Technologies Office (WWPTO). Sandia National Laboratories is a multi-program laboratory managed and operated by Sandia Corporation, a wholly owned subsidiary of Lockheed Martin Corporation, for the U.S. Department of Energy's National Nuclear Security Administration under contract DE-AC04-94AL85000.

CONTENTS

FIGURES

TABLES

NOMENCLATURE

CFSR	Climate Forecast System Reanalysis
DOE	Department of Energy
HWC	Humboldt WaveConnect
MHK	Marine and Hydrokinetic
NCEP	National Centers for Environmental Prediction
NETS	North Energy Test Site
NNMREC	Northwest National Maine Renewable Energy Center
PE	Percent error
PMEC	Pacific Marine Energy Center
RMSE	Root-mean-square-error
SI	Scatter index
SWAN	Simulating WAves Nearshore
SNL	Sandia National Laboratories
WWIII	WAVEWATCH III
WEC	Wave Energy Converter

1. INTRODUCTION

The Department of Energy (DOE) Marine and Hydrokinetic (MHK) Program identified a need to develop modeling capabilities for nearshore (continental shelf) wave climate hindcasting at wave energy converter (WEC) study sites. In addition, the application of wave climate models for wave resource characterization at study sites is recommended in the (draft) International Electrotechnical Commission Technical Specification (IEC 62600-101 TS) on Wave Energy Characterization (IEC TS) (Folley et al. 2012).

As point measurements, buoy observations used as historical datasets may not accurately predict the wave climate at the study site. They either may not be in close enough proximity to the study site to be representative of the wave climate; or they may have an insufficient period of record (POR) to accurately characterize the wave climate statistics. The POR can be especially important for characterizing extreme sea states, as well as normal sea states when inter-period climate oscillations occur on the order of a few years or decades (e.g., Wang & Swail 2001, Vimont 2004). A minimum POR of ten years is often recommended for characterizing normal sea states, and twenty years for extreme sea states. However, it is rare to find buoy observations that are both representative of the wave climate at the study site, and with PORs greater than ten years. Therefore, model hindcasts of the wave climate offer an attractive alternative for wave characterization.

Wave climate models have their own limitations. Even if a wave model captures all of the essential physics (e.g., wave growth, nonlinear interactions, and dissipation), accurate modeling is still dependent on model inputs (e.g., wind data sources), model calibration and validation, and the dependency of predictions on the spatial and temporal model resolution.

An assessment of the spatial variation of wave characteristics is particularly important when conducting wave characterization studies for wave energy converter (WEC) test sites and commercial WEC deployments. The national wave resource assessment (EPRI 2011), which was conducted to estimate the total ocean wave energy resource for the United States, covered large regions. Model grid sizes were necessarily large at 4 arc minutes, which is on the order of 5 km depending on latitude and longitude. As a result, spatial variations of the ocean wave resource at the scales of commercial WEC deployments were not captured. Finer resolution wave models, with grid sizes of 50-500 m, are recommended in the (draft) International Electrotechnical Commission Technical Specification (IEC 62600-101 TS) on Wave Energy Characterization.

The goal of this study was to investigate the spatial variability of wave characteristics at a potential Tier 1 WEC test site located offshore of Humboldt Bay, California (Figure 1). The Simulating WAves Nearshore (SWAN) model was used to generate a 10-year hindcast of wave spectra and bulk parameters at 1-hour intervals. Wave statistics of this hindcast were calculated and analyzed at selected locations within the model domain, including individual (hourly) parameters, along with averaged monthly and seasonal data. In addition, spectral output at selected points directly offshore of the connection point was analyzed to understand the spatial variability of the wave climate in an area directly offshore of the potential connection point.

2. SITE DESCRIPTION

The SWAN model domain is shown in Figure 1. It encompasses the footprint of the former Pacific Gas & Electric's (PG&E) pilot project test bed, the Humboldt WaveConnect (HWC) described by Dooher et al. (2011). This is also the location of a comprehensive wave characterization study by Dallman and Neary (2014). The onshore connection point for the HWC project was the PG&E Fairhaven Substation. There is another substation at the nearby former pulp mill facility which has been acquired by the Humboldt Bay Harbor Recreation and Conservation District, and connects to the same transmission lines as the Fairhaven Substation. Because these two substations are essentially co-located, there is one marking in Figure 1 to signify them. This is the most likely onshore connection point for a future test or deployment site, however it may occupy an area at a different depth than the HWC project, depending on the site requirements. The model domain lies predominantly over a sedimentary shelf with a gently sloping seabed consisting of sand and clay. The bathymetry has few irregularities, such as canyons, that could disturb the local wave field near the HWC site (Dooher et al. 2011), but the southwest corner of the SWAN domain includes Eel Canyon.

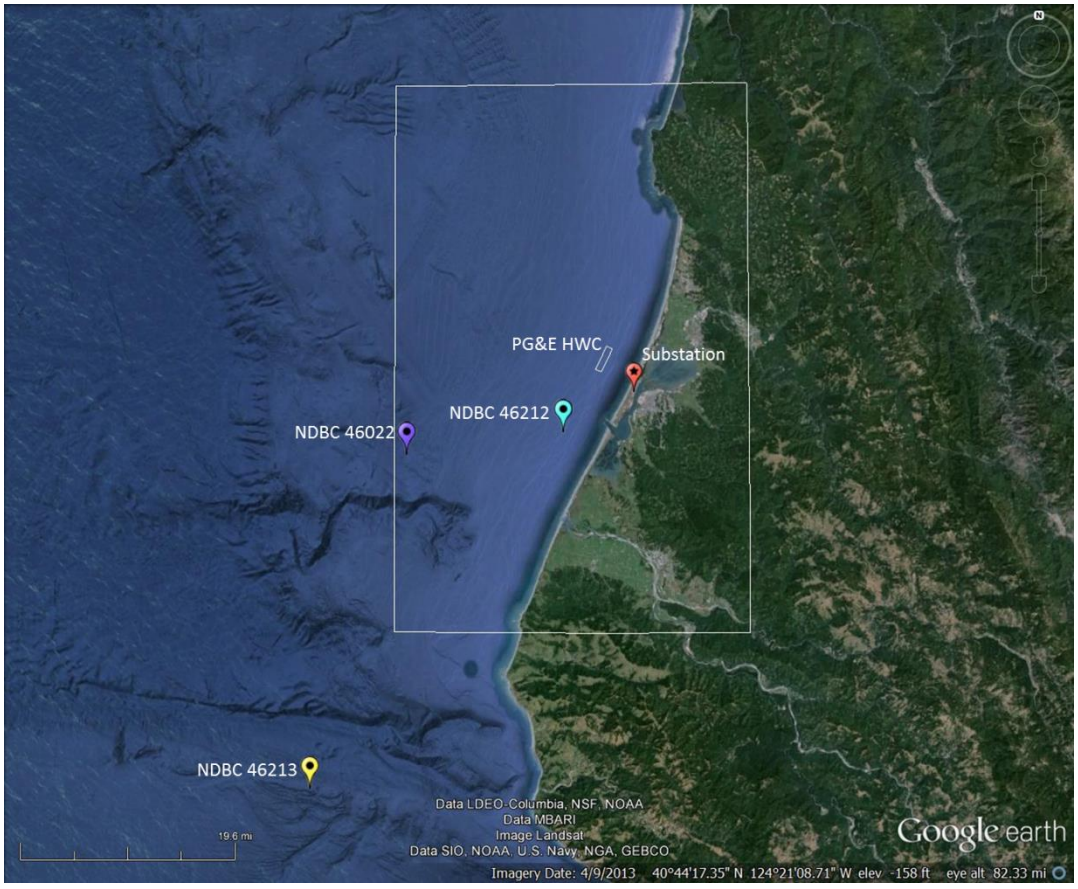

Figure 1. The SWAN domain (larger white box), NDBC46022, NDBC46212, and NDBC46213 buoys (purple, blue, and yellow thumbtacks), the PG&E Humboldt WaveConnect (HWC) array location (small white box), and the potential onshore substation site (red thumbtack) are shown.

The large scale WAVEWATCH III (Tolman 2009) model, v3.14, was implemented to establish the boundary conditions for the nearshore SWAN model (SWAN – User Manual 2013). Real-time wave data are available within the SWAN model domain from two buoys, NDBC46022 and NDBC46212/CDIP128. NDBC46213/CDIP094 is located outside the SWAN model domain, but is within the WWIII model domain. Buoy data is accessible online at the CDIP and NDBC databases. NDBC46022 is approximately 30 km southwest of the site, has been offline for repair and is expected to be operational in the fall of 2014. NDBC46212/CDIP128 is approximately 12 km from the test site, but was decommissioned in 2013. NDBC46213/ CDIP094 is approximately 75 km southwest of the site, and is still operational. Depth, POR, and location information for these buoys is summarized in Table 1. Throughout this report buoys will be referred to by their NDBC identifiers.

Table 1. Depth, POR, and location of the buoys used for performance metrics.

Buoy Identifier	Depth (m)	Years of Operation	Location
NDBC46212/CDIP128	**40**	**2004-2012**	**40.753 N 124.313 W (approximately 12 km southwest of the site)**
NDBC46022	**675**	**1996-present**	**40.724 N 124.578 W (approximately 30 km west/southwest of the site)**
NDBC46213/CDIP094	**334**	**2004-present**	**40.294 N, 124.7402W (approximately 75 km southwest of the site)**

3. METHODOLOGY

The large scale WAVEWATCH III (WWIII) (Tolman 2009) model, v3.14, was employed to establish boundary conditions for the nearshore SWAN model (SWAN – User Manual 2013). After a sensitivity study showed that a variety of nested grid sizes produced very similar performance metrics, three nested grids consisting of a global 1°, California coast 10', and a smaller California coast 2' grid were chosen for optimal run time. The WWIII model was forced with high resolution (0.5°) National Centers for Environmental Prediction (NCEP) Climate Forecast System Reanalysis (CFSR) wind data every 6 hours and ice data with resolution ~1.88° every 24 hours.

Output from the 2' WWIII grid along the boundaries of the SWAN domain, shown in Figure 1, was interpolated to set boundary conditions for the SWAN model. A grid sensitivity study concluded that 0.002° (~200 m) was the best grid size for the SWAN domain. Wind input was not used in SWAN because of the short fetch (García-Medina et al. 2013). In addition, ocean currents were not modeled or included as input data. The IEC TS on Wave Resource Characterization recommends including ocean current data in wave models if depth-averaged current speed exceeds 1.5 m/s. OSCAR satellite data near the test site is at 40.5 N, 125.5 W, and the 95th percentiles do not exceed 0.1 m/s. Although within Humboldt Bay there are currents up to 1 m/s during storm events (as measured by an ADCP during the Tsunami currents project, Admire et al. 2014), this area was not of interest for the current study which considered depths of 30 m or greater.

Breaking, friction, and triads were enabled in the SWAN model and default model parameters were used. The SWAN model results showed negligible sensitivity to variations in calibration parameters for the friction and whitecapping submodels at depths of about 30 m or greater.

For the purpose of investigating the spatial variation of wave statistics, spectral output from the SWAN domain was saved at points directly offshore from the substation (Figure 2). From this spectral output, the six IEC TS parameters can be calculated (omnidirectional wave power J, significant wave height H_{m0}, energy period T_e, spectral width ϵ_0, direction of maximally resolved wave power θ, and directionality coefficient d_θ. Various bulk parameters (significant wave height H_{m0}, energy period T_e, peak period T_p, peak wave direction D_p) were calculated by SWAN and saved over the entire domain.

Initially one year of hindcast data was used to validate both the WWIII and SWAN models. The following model performance metrics were computed to quantify the discrepancies between bulk wave parameters derived by model simulations and those derived by buoy measurements. The root-mean-square-error (*RMSE*) is defined as

$$RMSE = \sqrt{\frac{\sum_{i=1}^{N}(M_i - P_i)^2}{N}}$$

where N is the number of observations, M_i is the measured value, and P_i is the predicted value. The percent error (*PE*) is

$$PE = 100\sqrt{\frac{1}{N}\sum_{i=1}^{N}\left(\frac{M_i - P_i}{M_i}\right)^2},$$

the scatter index (*SI*) is

$$SI = \frac{RMSE}{\bar{M}},$$

where the overbar indicates the mean, the bias is

$$Bias = \frac{1}{N}\sum_{i=1}^{N}(P_i - M_i),$$

and the linear correlation coefficient, R, is

$$R = \frac{\sum_{i=1}^{N}(M_i - \bar{M})(P_i - \bar{P})}{\sqrt{(\sum_{i=1}^{N}(M_i - \bar{M})^2)(\sum_{i=1}^{N}(P_i - \bar{P})^2)}}.$$

The *RMSE* and bias can also be expressed as percentages relative to the measured dataset. A positive value of bias indicates an overprediction by the model, and a negative bias indicates an underprediction.

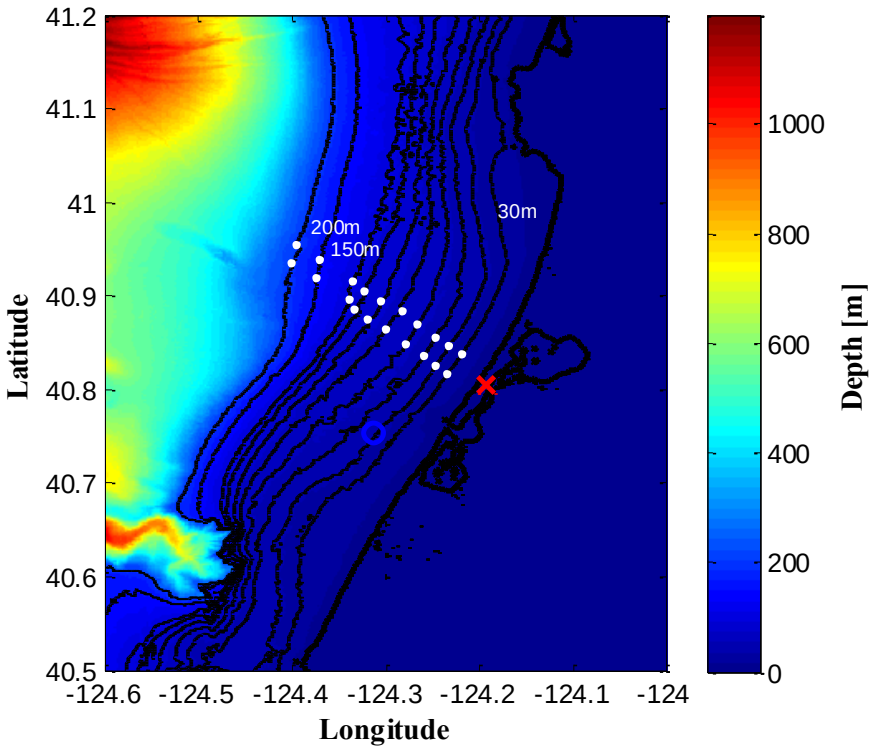

Figure 2. The depth over the SWAN domain is shown. The white dots are spectral output locations, the onshore connection point is marked as a red x, and the location of NDBC46212 buoy is marked as an open circle. Depth contours are shown every 10 m from 30-100 m, along with the 100 m and 150 m contours.

4. MODEL RESULTS

4.1. Model Validation

For model validation, the six IEC TS parameters generated from the SWAN hindcast data from January 1, 2008 through December 31, 2008 were compared to those from measured data from NDBC46212. Comparisons of the time histories of the IEC TS parameters calculated from the hindcast and buoy observations are shown in the Appendix in Figure 11. Generally, the model predicts the temporal pattern of the buoy-derived values, but significant discrepancies are observed at a few points in time, e.g., the peak in H_{m0} on January 16 that is not captured by the model. A possible explanation for these discrepancies is the temporal resolution of the wind data (6 hour intervals) which leads to underprediction of high winds.

The computed performance metrics for each variable of interest (omnidirectional wave power J, significant wave height H_{m0}, energy period T_e, spectral width ϵ_0, direction of maximally resolved wave power θ, and directionality coefficient d_θ) are shown in Table 2. Values of *RMSE* and *PE* are less than 20%, except those for the omnidirectional wave power, which are multiplied because wave power is proportional to the wave height squared and energy period. The correlations are very high, near 0.9 for all variables except spectral width and directionality coefficient, which are somewhat lower. The significant wave height, H_{m0}, is overpredicted in the model by about 6%, while the energy period, T_e, is slightly underpredicted. Note that although H_{m0} is in general overpredicted, it is clear by visual inspection that smaller wave heights are usually overpredicted while some of the larger wave heights are slightly underpredicted. The poor performance of wave models predicting large waves, specifically underpredicting wave heights, has been reported by others (e.g., Forte et al. 2012, Chawla et al. 2013), and has raised concerns when using hindcasts to estimate extreme events.

Table 2. The model performance metrics for SWAN for the year 2008 at NDBC46212 are shown for omnidirectional wave power J, significant wave height H_{m0}, energy period T_e, spectral width ϵ_0, direction of maximally resolved wave power θ, and directionality coefficient d_θ.

	RMSE	RMSE (%)	PE	SI	Bias	Bias (%)	R
J	18.1 kW/m	60%	52%	0.60	5.3 kW/m	17.6%	0.92
H_{m0}	0.39 m	18%	19%	0.18	0.13 m	6.3%	0.93
T_e	0.76 s	8%	8%	0.08	-0.12 s	-1.3%	0.92
ϵ_0	0.05	15%	14%	0.15	-0.01	-4.0%	0.76
θ	8.2 °	3%	3%	0.03	-3.2 °	-1.0%	0.93
d_θ	0.07	8%	12%	0.08	0.05	5.2%	0.60

Values for model performance metrics in Table 2 are similar or better than those reported for resource assessments in the literature (van Nieuwkoop et al. 2013, Arinaga & Cheung 2012, García-Medina et al. 2014). The common performance metrics reported in van Nieuwkoop et al. (2013) include H_{m0} and T_e, and the *SI* and Bias were approximately 0.17 and -4% for H_{m0}, and 0.24 and -18% for T_e. For H_{m0}, this is similar to the present results, however their H_{m0} had slightly lower (and negative) bias while their T_e had a much higher SI and larger negative bias. Arinaga & Cheung (2012) reported performance metrics for H_{m0} and the peak period, T_p. For the buoys in shallow water (72 and 80 m), the *RMSE* was 0.20-0.38 m and R was 0.92-0.95 for H_{m0}, which is similar to the present results. The *RMSE* was 1.8-4.2 s and R was 0.57-0.65 for T_p, which is a larger *RMSE* and lower correlation than the present results for T_e. García-Medina et al. (2014) reported performance metrics for the same variables shown in Table 2, and are listed in the Appendix in Table 10 for reference. All metrics were similar to the present results. In particular, the present RMSE, PE, and SI were slightly lower than García-Medina et al. for H_{m0} and T_e, while the bias was higher for H_{m0} and lower for T_e.

The performance statistics for WWIII were also evaluated to assess its performance and ensure that the overbias of wave height in SWAN was based on the quality of the input data (from WWIII). The WWIII hindcast data from January 1, 2008 through December 31, 2008 was compared to measured data from NDBC46022 and NDBC46213. The bulk parameters significant wave height, H_{m0}, and peak period, T_p, were saved at these buoy locations. The computed performance statistics for each parameter are shown in Table 3 for NDBC46022 and Table 4 for NDBC46213. From these performance statistics, it is clear that the wave height in WWIII is overbiased as well, and at the same order of magnitude as the overbias in SWAN. This bias originates from the CFSR winds that are used to drive WWIII. Previous studies have found a similar bias in the winds, the magnitude of which depends on location and season (e.g., Stopa & Cheung 2014, Forte et al. 2012, Ardhuin et al. 2011, Rogers et al. 2012). In version 4.18 of WWIII (released in March 2014), which was released after this study, the manual recommends adjusting the wind-wave growth parameter 'BETAMAX' to account for the bias in CFSR winds (Tolman 2014). This recommendation will be implemented in future versions of the model used in this study.

Table 3. Performance metrics for WWIII for the year 2008 at NDBC46022.

	RMSE	RMSE (%)	PE	SI	Bias	Bias (%)	R
H_{m0}	0.49 m	21%	18%	0.21	0.25 m	10.8%	0.93
T_p	2.09 s	19%	20%	0.19	-0.28 s	-2.5%	0.71

Table 4. Performance metrics for WWIII for the year 2008 at NDBC46213.

	RMSE	RMSE (%)	PE	SI	Bias	Bias (%)	R
H_{m0}	0.45 m	18%	16%	0.18	0.19 m	7.5%	0.93
T_p	2.28 s	20%	23%	0.20	-0.41 s	-3.6%	0.69

The 10-year hindcast (January 2000 – December 2009) for Humboldt Bay, CA was completed, and performance metrics were computed to quantify the model's performance. The overlapping years of operation of NDBC46212 are 2004-2009. The performance metrics described above are shown in Table 5 for the period 2004-2009. These values are very similar to Table 2, confirming that the validation of the model over the year 2008 was representative of the full length of buoy data, and adds confidence that the model can be used to extend hindcasts for multiple years. The WWIII performance metrics over the whole range of buoy data available are shown in Table 6 and Table 7.

Table 5. The SWAN performance metrics for the years 2004-2009 at NDBC46212 are shown for omnidirectional wave power J, significant wave height H_{m0}, energy period T_e, spectral width ϵ_0, direction of maximally resolved wave power θ, and directionality coefficient d_θ.

	RMSE	RMSE (%)	PE	SI	Bias	Bias (%)	R
J	17.1 kW/m	58%	52%	0.58	5.0 kW/m	17.1%	0.92
H_{m0}	0.37 m	18%	19%	0.18	0.11 m	5.5%	0.93
T_e	0.83 s	9%	9%	0.09	-0.14 s	-1.5%	0.92
ϵ_0	0.05	15%	14%	0.15	-0.01	-3.39%	0.75
θ	8.0 °	3%	3%	0.03	-2.1 °	-0.71%	0.92
d_θ	0.07	8%	14%	0.08	0.05	5.24%	0.56

Table 6. Performance metrics for WWIII for the years 2004-2009 at NDBC46022.

	RMSE	RMSE (%)	PE	SI	Bias	Bias (%)	R
H_{m0}	0.46 m	19%	17%	0.19	0.17 m	7.0%	0.92
T_p	2.22 s	20%	20%	0.20	-0.07 s	-0.7%	0.71

Table 7. Performance metrics for WWIII for the years 2004-2009 at NDBC46213.

	RMSE	RMSE (%)	PE	SI	Bias	Bias (%)	R
H_{m0}	0.44 m	18%	16%	0.18	0.18 m	7.1%	0.93
T_p	2.25 s	19%	24%	0.19	-0.49 s	-4.2%	0.72

4.2. Spatial Variation of Bulk Parameters in Model Domain

To evaluate the spatial variability of wave characteristics, contour plots of the average significant wave height for each season are shown in Figure 3 with the same color scales (to emphasize seasonal variability) and Figure 4 with different color scales (to emphasize the spatial variation for each season). As mentioned in the Methodology, hindcast output of the bulk parameters H_{m0}, T_e, T_p, and D_p were saved over the domain at each 1-hour time step. These values were averaged over the four seasons at each point. In these plots, spring is defined as March – May, summer as June – August, fall as September – November, and winter as December – February. The wave heights at depths of 15 m or less have been zeroed and appear as dark blue. The axes have 0.1 decimal degree increments (~10 km). As shown in Figure 3, spring and fall have similar significant wave heights ranging from approximately 2 – 2.5 m. Summer has lower significant wave heights between 1.5 – 2 m. Winter has much larger significant wave heights well over 2.5 m over the majority of the domain.

In order to show how the wave field may vary at individual time steps compared to a seasonal average, contours at one instance in time for winter are shown in Figure 5 and for summer in Figure 6. The contour plot at 16:00 on February 12, 2008 (Figure 5) is representative of the average winter value for significant wave height, while the contour plot at 11:00 on July 25, 2008 (Figure 6) is representative of the average summer value.

In the winter (Figure 4 bottom right), the contours of significant wave height align well with the depth contours as they approach the shore. Significant wave height along each depth contour line of 100 m or less is fairly constant. This is particularly evident for the area directly offshore (perpendicular) of the potential onshore connection point (marked by an X in Figure 3 and Figure 4). As an example, the Northwest National Marine Renewable Energy Center (NNMREC) Pacific Marine Energy Center (PMEC) North Energy Test Site (NETS) is 1 square nautical mile (~1.85 km). The distance from the 40 m to 50 m contour lines directly offshore of the connection point in Figure 3 is approximately 1.75 km. If a potential test site offshore of Humboldt Bay was the same size as NETS and oriented parallel to the depth contours, it would span from the 40 m to 50 m depths. This would result in a spatial variation of significant wave height of about 0.1 m in the perpendicular (northwest to southeast) direction, with very little variation in the direction parallel to the depth contours. The HWC site is approximately 0.93 km in width (approximately perpendicular to the shoreline) and 3.71 km in length (parallel to the shoreline). Therefore, it also has little spatial variation of significant wave height in the perpendicular direction (less than 0.1 m). Because the wave heights are nearly constant along the contours at this location, the difference is negligible in the parallel direction.

In the summer (Figure 4 top right), there is more variation of wave height along the depth contours. Summer waves are dominated by winds from the north/northeast, and as seen in Figure 7, the peak wave direction is generally from northeast (around 300°). Figure 8 shows the coastline north of Humboldt Bay, which is characterized by land protruding to the west in the northeast edge of the SWAN domain (Trinidad, CA), and land protruding further to the west in southern Oregon. This causes sheltering of the north/northeasterly winds (and therefore waves) during the summer. In the southern part of the SWAN domain (around 40.5 N), the waves begin to clear and the heights are larger. Despite the variation across depth contours, the significant

wave height variation across a potential 1 nautical mile test site situated between the 40 m and 50 m depth contours would be less than 0.1 m, similarly to the winter.

The topography of the ocean floor often causes interesting effects on the waves. For example García-Medina et al. (2014) showed that canyons, banks, and sea stacks affect the wave transformation depending on incoming wave direction. In this study, an interesting observation is the effect of Eel Canyon on the waves in the southern part of the domain (around 40.6 - 40.7 N). The 200 m depth contour curves sharply towards the coast (see Figure 2) due to the underwater canyon formation, creating a very steep bottom slope. The large deep water waves appear to fan out around the canyon, causing relatively higher significant wave heights just north and south of the canyon near the shore. This is most evident in the winter (Figure 4) when the peak wave direction is from west/northwest (Figure 7).

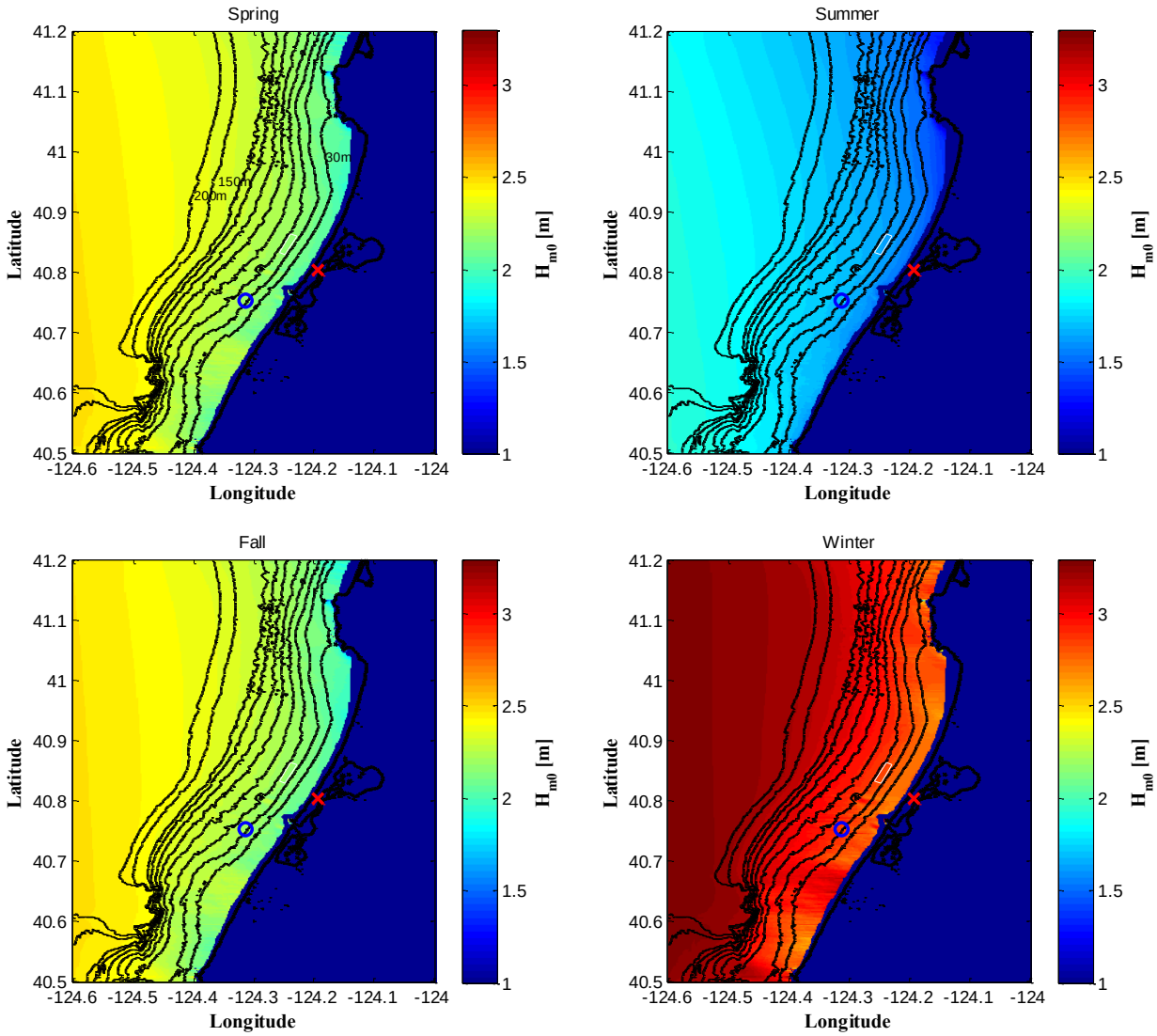

Figure 3. The average significant wave height over the domain is shown for each season. The same color bar has been used to emphasize the seasonal variability. The onshore connection point is marked as a red x, the location of the NDBC46212 buoy as an open blue circle, and the HWC location is outlined in white. Several depth contours are shown, and are labeled in the top left figure.

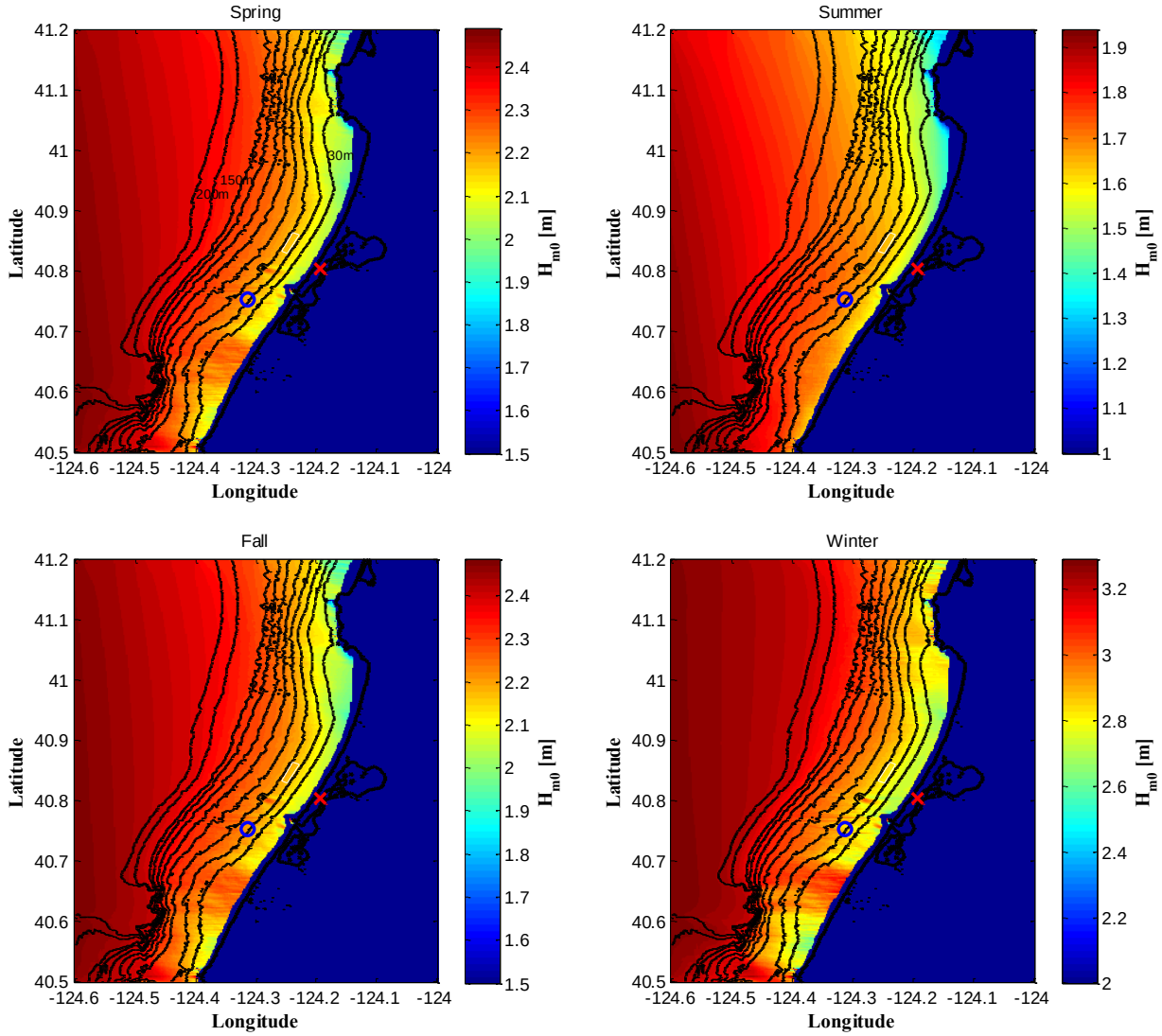

Figure 4. The average significant wave height over the domain is shown for each season. Each season has a different color bar to emphasize the variability over the domain. The onshore connection point is marked as a red x, the location of the NDBC46212 buoy is marked as an open blue circle, and the HWC location is outlined in white. Several depth contours are shown, and are labeled in the Spring (top left) figure.

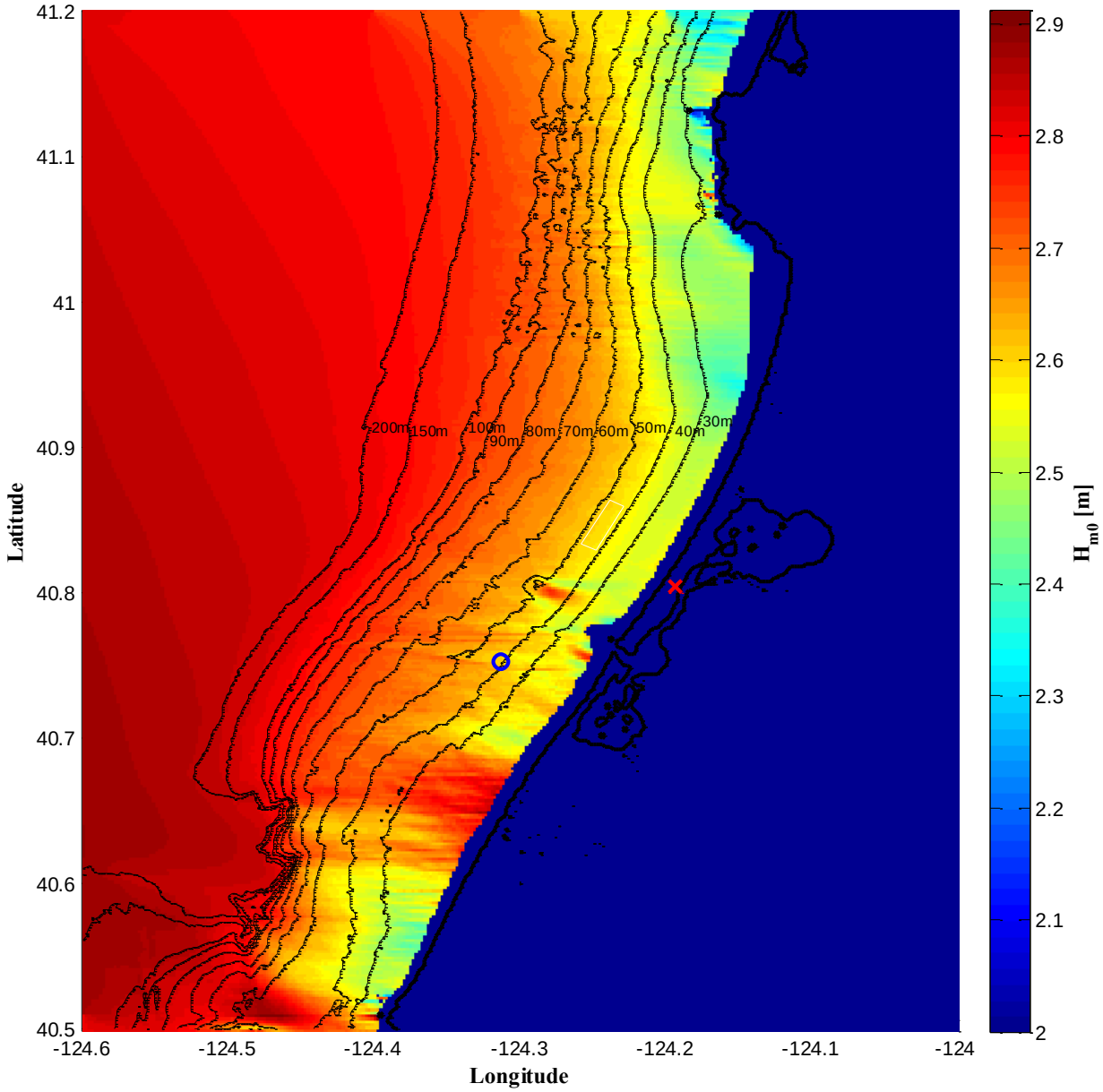

Figure 5. Spatial variation of the significant wave height, H_{m0}, over the model domain on February 12, 2008 at 16:00.

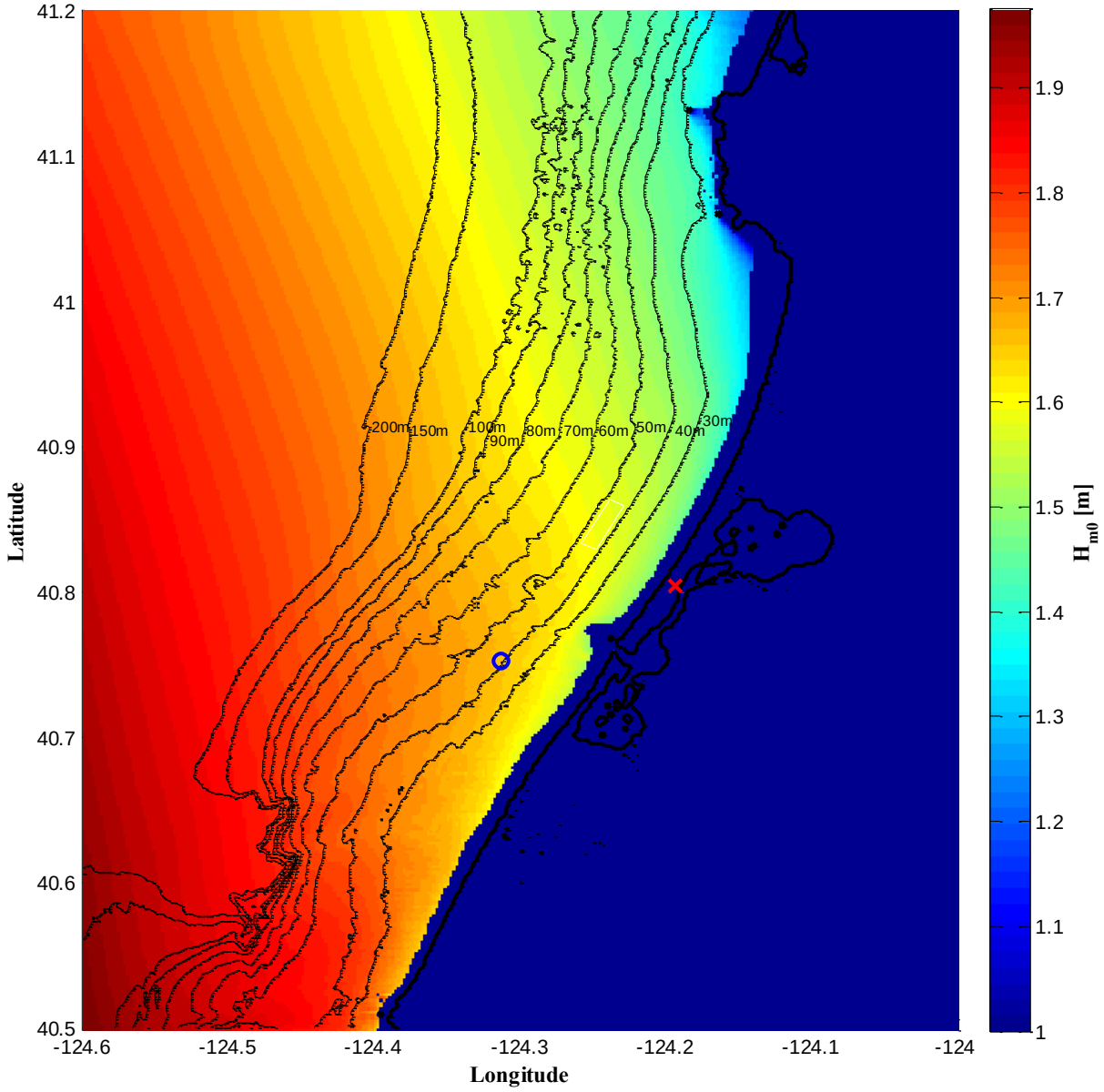

Figure 6. Spatial variation of the significant wave height, H_{m0}, over the model domain on July 25, 2008 at 11:00.

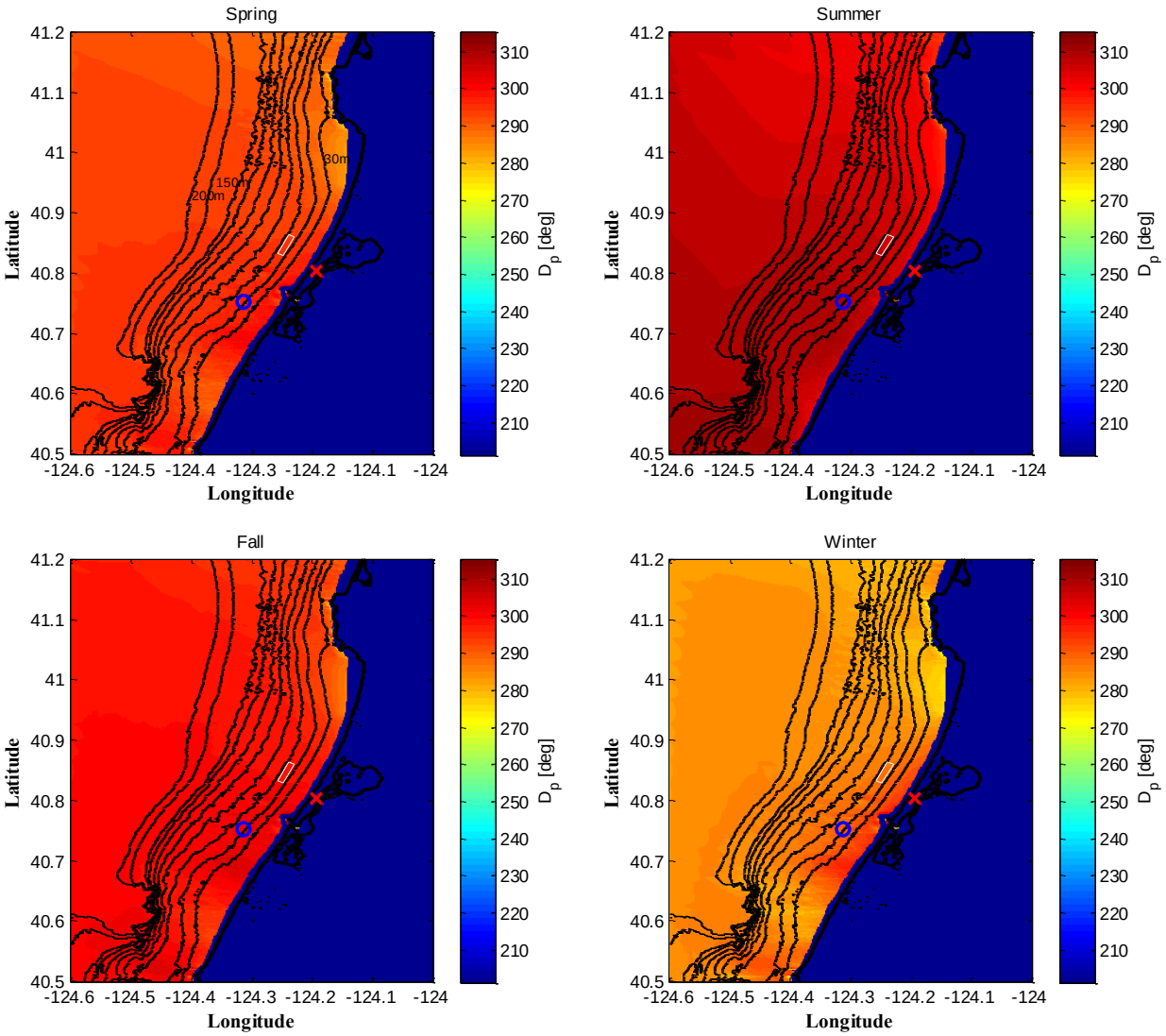

Figure 7. The average of the peak wave direction, D_p, over the domain is shown for each season. The same color bar has been used in all seasons to emphasize the seasonal variability. Depth contours are shown every 10 m from 30-100 m, along with the 100 m and 150 m contours.

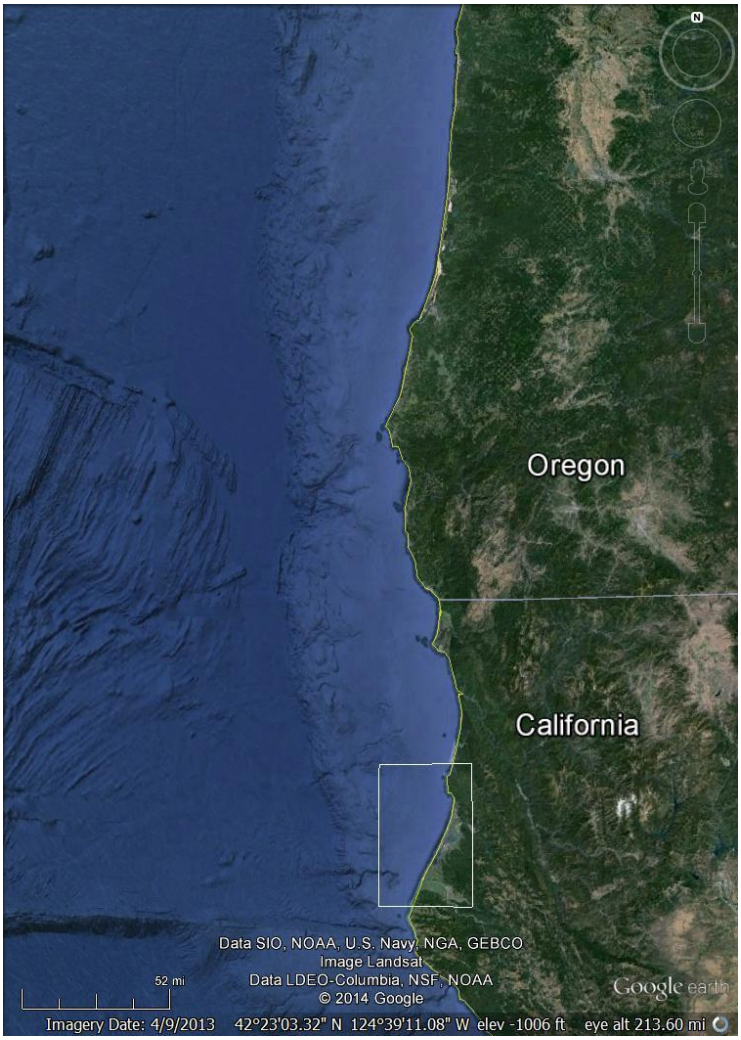

Figure 8. Image of the coastline of the U.S. Pacific Northwest coast. Note the features in Southern Oregon and in the northeast corner of the SWAN domain (white box) where the coastline protrudes to the west.

4.3. Spatial Variation of Data at Spectral Output Points

It is clear from Section 4.2 that there is little variation in the wave characteristics between the two points on each contour line, so the following analyses use the average data between each pair on the contours. Monthly averages of the six IEC TS parameters, omnidirectional wave power J, significant wave height H_{m0}, energy period T_e, spectral width ϵ_0, direction of maximally resolved wave power θ, and directionality coefficient d_θ are shown in Figure 9 and Figure 10. The values at the 40 m depth contour, offshore of the substation (Figure 1) are shown in Figure 9, and the values at the 80 m depth contour are shown in Figure 10. Overall the monthly variation in parameters is similar at the two depths. Winter months are characterized by larger J, H_{m0}, and T_e, with more variation (larger spread between 5th and 95th percentiles) than the summer months. These three parameters are slightly larger at the 80 m depth, and the values are reported in Tables 8 and 9. As found in Garcia-Medina et al. 2014, the directional spread of wave power narrows (indicated by larger directionality coefficient, d_θ) with decreasing depth. This is apparent in comparing Figure 9 and Figure 10, where the 80 m depth location has a larger spread and lower values of d_θ than the 40 m depth, where the directionality has narrowed.

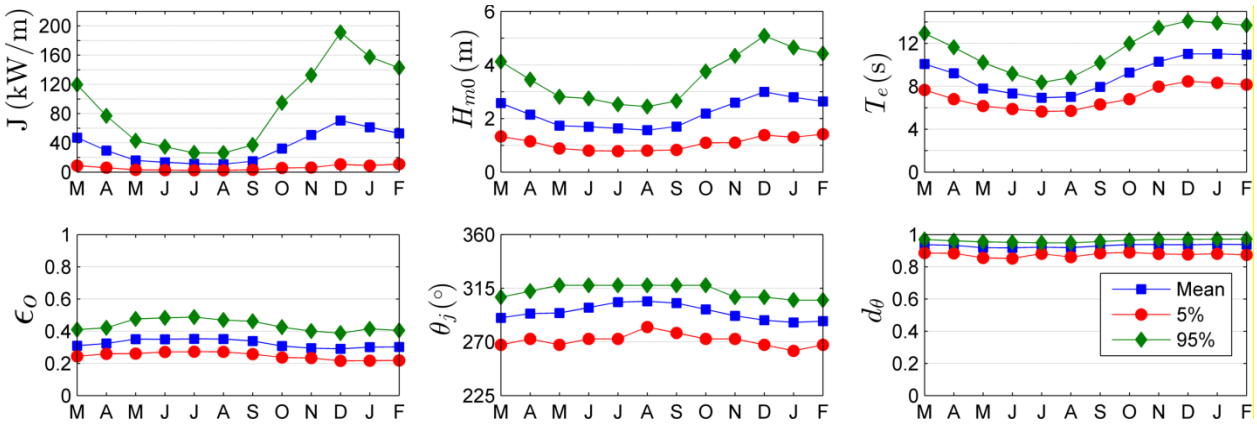

Figure 9. Monthly averages of the six parameters of interest at the 40 m depth contour, offshore of the substation.

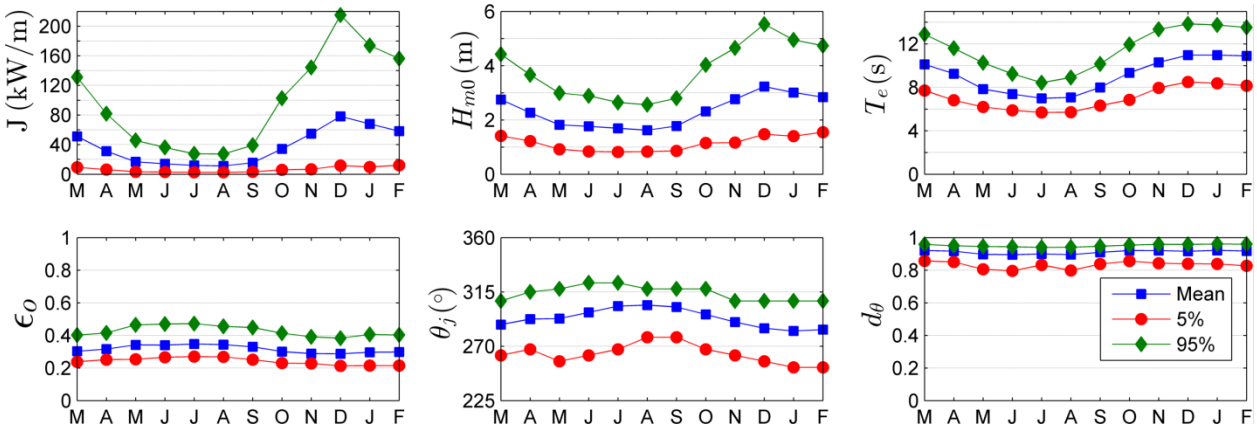

Figure 10. Monthly averages of the six parameters of interest at the 80 m depth contour, offshore of the substation.

Table 8. The average, 5th and 95th percentiles of the six parameters at the 40 m depth (see Figure 9).

	$J\ [kW/m]$			$H_{m0}\ [m]$			$T_e\ [s]$		
	5%	**Mean**	**95%**	**5%**	**Mean**	**95%**	**5%**	**Mean**	**95%**
March	8.8	47.1	119.6	1.33	2.57	4.12	7.65	10.08	12.94
April	5.9	29.5	76.9	1.15	2.14	3.45	6.81	9.21	11.64
May	3.1	15.8	42.8	0.88	1.73	2.81	6.16	7.80	10.22
June	2.8	13.4	34.7	0.80	1.69	2.75	5.88	7.33	9.18
July	2.4	11.3	26.2	0.78	1.63	2.52	5.65	6.93	8.36
August	2.4	10.7	26.0	0.80	1.56	2.44	5.71	7.02	8.81
September	3.1	14.9	37.1	0.83	1.70	2.65	6.31	7.94	10.20
October	5.6	32.1	94.7	1.09	2.19	3.75	6.80	9.28	11.99
November	6.2	50.8	132.5	1.10	2.59	4.33	7.97	10.30	13.46
December	10.7	70.6	191.0	1.38	2.99	5.08	8.46	11.02	14.09
January	8.8	61.3	157.4	1.30	2.79	4.65	8.32	11.02	13.93
February	11.0	53.0	142.6	1.41	2.63	4.42	8.15	10.96	13.69

	ϵ_0			$\theta_j\ [°]$			d_θ		
	5%	**Mean**	**95%**	**5%**	**Mean**	**95%**	**5%**	**Mean**	**95%**
March	0.24	0.31	0.41	267.5	290.1	307.5	0.89	0.94	0.97
April	0.26	0.32	0.42	272.5	293.7	312.5	0.88	0.93	0.96
May	0.26	0.35	0.48	267.5	294.2	317.5	0.86	0.92	0.95
June	0.27	0.35	0.48	272.5	298.8	317.5	0.85	0.92	0.95
July	0.27	0.35	0.49	272.5	303.3	317.5	0.88	0.92	0.95
August	0.27	0.35	0.47	282.5	304.1	317.5	0.86	0.92	0.95
September	0.26	0.34	0.46	277.5	302.5	317.5	0.88	0.93	0.96
October	0.24	0.31	0.42	272.5	297.2	317.5	0.89	0.94	0.96
November	0.23	0.29	0.40	272.5	291.8	307.5	0.88	0.94	0.97
December	0.22	0.29	0.39	267.5	288.2	307.5	0.88	0.94	0.97
January	0.22	0.30	0.41	262.5	286.3	305.0	0.88	0.94	0.97
February	0.22	0.30	0.40	267.5	287.4	305.0	0.87	0.94	0.97

Table 9. The average, 5th and 95th percentiles of the six parameters at the 80 m depth (see Figure 10).

	$J\ [kW/m]$			$H_{m0}\ [m]$			$T_e\ [s]$		
	5%	**Mean**	**95%**	**5%**	**Mean**	**95%**	**5%**	**Mean**	**95%**
March	9.3	51.1	131.1	1.41	2.75	4.42	7.71	10.11	12.89
April	6.3	31.1	81.8	1.22	2.26	3.66	6.81	9.26	11.60
May	3.2	16.7	45.7	0.92	1.82	2.99	6.20	7.85	10.26
June	2.9	14.1	36.1	0.84	1.76	2.89	5.89	7.38	9.24
July	2.6	11.9	27.5	0.82	1.69	2.64	5.68	6.99	8.42
August	2.6	11.2	27.3	0.83	1.62	2.56	5.72	7.07	8.91
September	3.2	15.5	39.1	0.86	1.77	2.80	6.32	7.99	10.15
October	5.9	34.2	102.7	1.15	2.32	4.03	6.86	9.34	11.95
November	6.6	54.8	144.2	1.16	2.76	4.65	7.95	10.31	13.34
December	11.7	78.2	214.9	1.47	3.23	5.53	8.50	10.97	13.84
January	9.7	67.9	173.9	1.40	3.01	4.95	8.37	10.97	13.75
February	12.1	58.2	156.2	1.55	2.84	4.74	8.15	10.90	13.53

	ϵ_0			$\theta_j\ [°]$			d_θ		
	5%	**Mean**	**95%**	**5%**	**Mean**	**95%**	**5%**	**Mean**	**95%**
March	0.24	0.30	0.40	262.5	288.0	307.5	0.86	0.92	0.96
April	0.25	0.32	0.41	267.5	292.5	315.0	0.85	0.92	0.95
May	0.25	0.34	0.46	257.5	292.9	317.5	0.81	0.90	0.95
June	0.27	0.34	0.47	262.5	298.0	322.5	0.80	0.90	0.94
July	0.27	0.35	0.47	267.5	303.2	322.5	0.83	0.90	0.94
August	0.27	0.34	0.46	277.5	304.1	317.5	0.80	0.90	0.94
September	0.25	0.33	0.45	277.5	302.6	317.5	0.84	0.91	0.95
October	0.23	0.30	0.41	267.5	296.4	317.5	0.86	0.92	0.95
November	0.23	0.29	0.39	262.5	290.0	307.5	0.84	0.92	0.96
December	0.21	0.29	0.38	257.5	284.9	307.5	0.84	0.92	0.96
January	0.21	0.30	0.41	252.5	282.7	307.5	0.84	0.92	0.96
February	0.21	0.30	0.40	252.5	283.8	307.5	0.83	0.92	0.96

4. SUMMARY AND CONCLUSIONS

Time histories of the bulk wave parameters derived by model simulations were compared to those derived by buoy measurements from NDBC 46212 for the year 2008. Based on visual inspection of time histories of the bulk wave parameters and model performance metrics, the model performed as well as other SWAN models reported in the literature.

The 10-year hindcast was completed (January 2000 – December 2009), and performance metrics over the period 2004-2009 were very close to those considered for the validation of one year. In general, the significant wave height was slightly overpredicted, which led to an overprediction of the omnidirectional wave power density. This is important to note for resource characterization. The overprediction of wave height also occurred in WWIII, which was used as boundary conditions to the SWAN model. The overprediction is due to the overbias in CFSR wind data which has been reported in the literature.

An assessment of spatial variation showed that the amount of variation along depth contours depends on the season. The variation in wave height along depth contours was higher in the summer due to the wind and wave sheltering from the protruding land on the coastline north of the model domain. However, the spatial variation along an assumed typical test site of 1 square nautical mile is almost negligible; at most about 0.1 m in both winter and summer. The six wave characterization parameters were calculated at several points directly offshore of the substation. The parameters varied with depth but showed very similar trends.

Although limited to the wave climate offshore of Humboldt Bay, the results of this study suggest that a 200 m grid is more than sufficient to capture the spatial variation of wave statistics. A smaller grid size, such as 50 m, recommended in the IEC TS for a ‘design’ characterization is not necessary unless a study includes device interaction, where typically the grid cell would be the same size (or less) than a device diameter.

5. REFERENCES

Admire AR, Dengler LA, Crawford GB, Burak UU, Borrero JC, Greer SD, Wilson RI (2014) Observed and Modeled Currents from the Tohoku-oki, Japan and other Recent Tsunamis in Northern California. *Pure Appl Geophys*, Published online February 2014.

Ardhuin F, Hanafin J, Quilfen Y, Chapron B, Queffeulou P, Obrebski M (2011) Calibration of the "IOWAGA" Global Wave Hindcast (1991-2011) Using ECMWF and CFSR Winds. *Proceedings of the 12th International Workshop on Wave Hindcasting and Forecasting*, Kohala Coast, Hawaii.

Arinaga RA, Cheung KF (2012) Atlas of global wave energy from 10 years of reanalysis and hindcast data. *Renew Energy* 39:49-64.

Chawla A, Spindler DM, Tolman HL (2013) Validation of a thirty year wave hindcast using the Climate Forecast System Reanalysis Winds. *Ocean Model* 70:189-206.

Dallman AR, Neary VS (2014) Characterization of U.S. Wave Energy Converter (WEC) Test Sites: A Catalogue of Met-Ocean Data. SAND2014-18206, Sandia National Laboratories, Albuquerque, NM.

Electric Power Research Institute (EPRI) (2011). Mapping and Assessment of the United States Ocean Wave Energy Resource. *EPRI 2011 Technical Report to U.S. Department of Energy.*

Folley M, Cornett A, Holmes B, Lenee-Bluhm P, Liria P (2012) Standardising resource assessment for wave energy converters. *Proceedings of the 4th Annual International Conference on Ocean Energy*, Dublin.

Forte MF, Hanson JL, Hagerman G (2012) North Atlantic Wind and Wave Climate: Observed Extremes, Hindcast Performance, and Extratropical Recurrence Intervals. *Proceedings of the OCEANS 2012 IEEE Conference*, Hampton Roads, Virginia.

García-Medina G, Özkan-Haller HT, Ruggiero P, Oskamp J (2013) An Inner-Shelf Wave Forecasting System for the U.S. Pacific Northwest. *Weather and Forecasting* 28:681-703.

García-Medina G, Özkan-Haller HT, Ruggiero P (2014) Wave resource assessment in Oregon and southwest Washington, USA. *Renew Energy* 64:203-214.

Rogers WE, Dykes JD, Wang D (2012) Validation Test Report for WAVEWATCH III. Naval Research Laboratory Report NRL/MR/7320--12-9425.

Stopa JE, Cheung KF (2014) Intercomparison of wind and wave data from the ECMWF Reanalysis Interim and the NCEP Climate Forecast System Reanalysis. *Ocean Model* 75:65-83.

SWAN – User Manual. Delft University of Technology, Environmental Fluid Mechanics Section, available from *http://www.swan.tudelft.nl (*Version 40.91ABC, 2013).

Tolman H. User manual and system documentation of WAVEWATCH III version 3.14, available from *http://polar.ncep.noaa.gov/waves/wavewatch/* (Version 3.13, 2009).

Tolman H. User manual and system documentation of WAVEWATCH III version 4.18, available from *http://polar.ncep.noaa.gov/waves/wavewatch/* (Version 4.18, 2014).

van Nieuwkoop JCC, Smith HCM, Smith GH, Johanning L (2013) Wave resource assessment along the Cornish coast (UK) from a 23-year hindcast dataset validated against buoy measurements. *Renew Energy* 58:1-14.

Vimont DJ (2004) The Contribution of the Interannual ENSO Cycle to the Spatial Pattern of Decadal ENSO-Like Variability. Journal of Climate 18:2080-2092.

Wang XL, Swail VR (2001) Changes of Extreme Wave Heights in Northern Hemisphere Oceans and Related Atmospheric Circulation Regimes. *Journal of Climate* 14:2204-2221.

APPENDIX

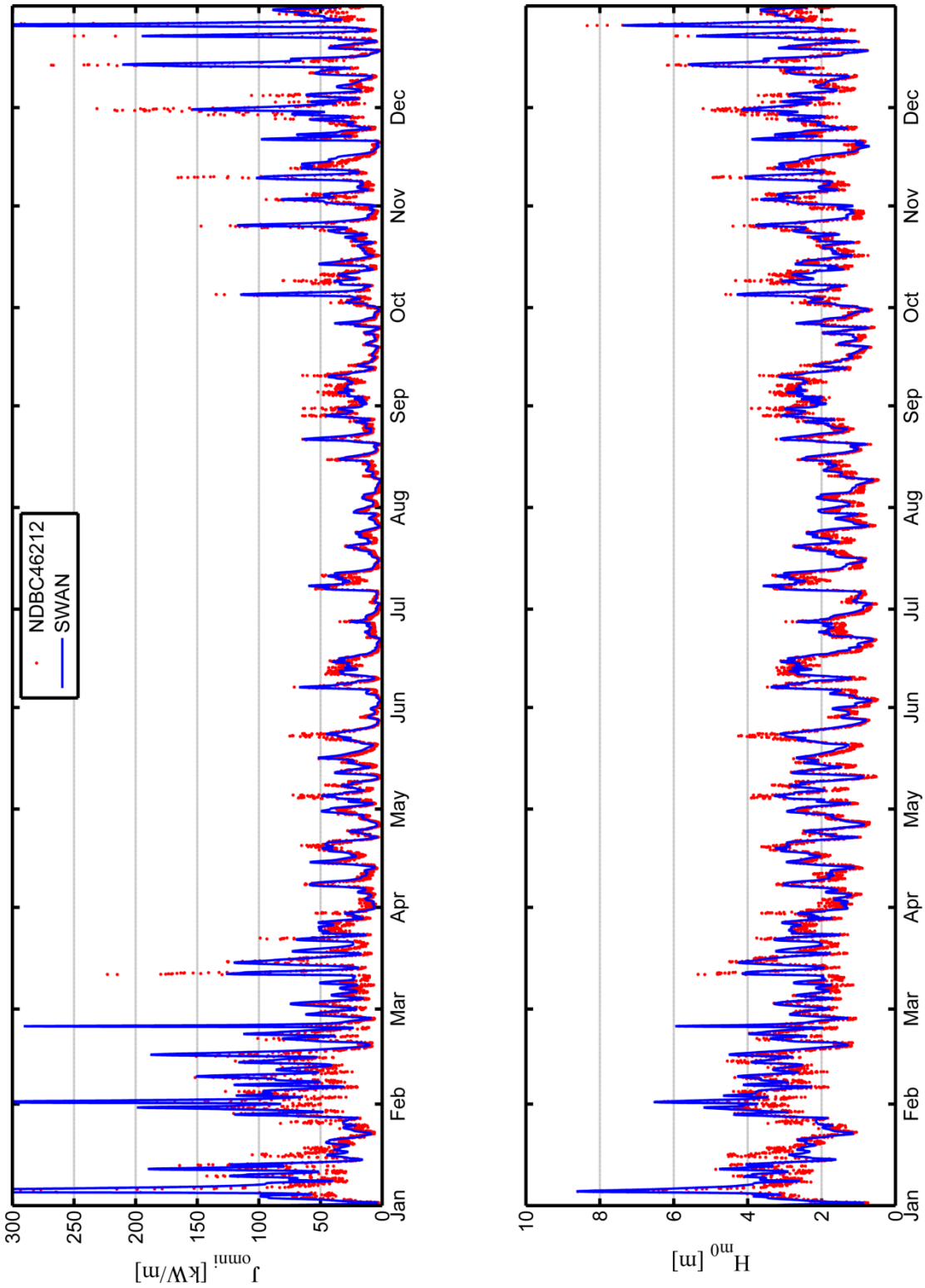
NDBC46212
SWAN
J_{omni} [kW/m]
H_{m0} [m]
0
50
100
150
200
250
300
0
2
4
6
8
10
Jan
Feb
Mar
Apr
May
Jun
Jul
Aug
Sep
Oct
Nov
Dec

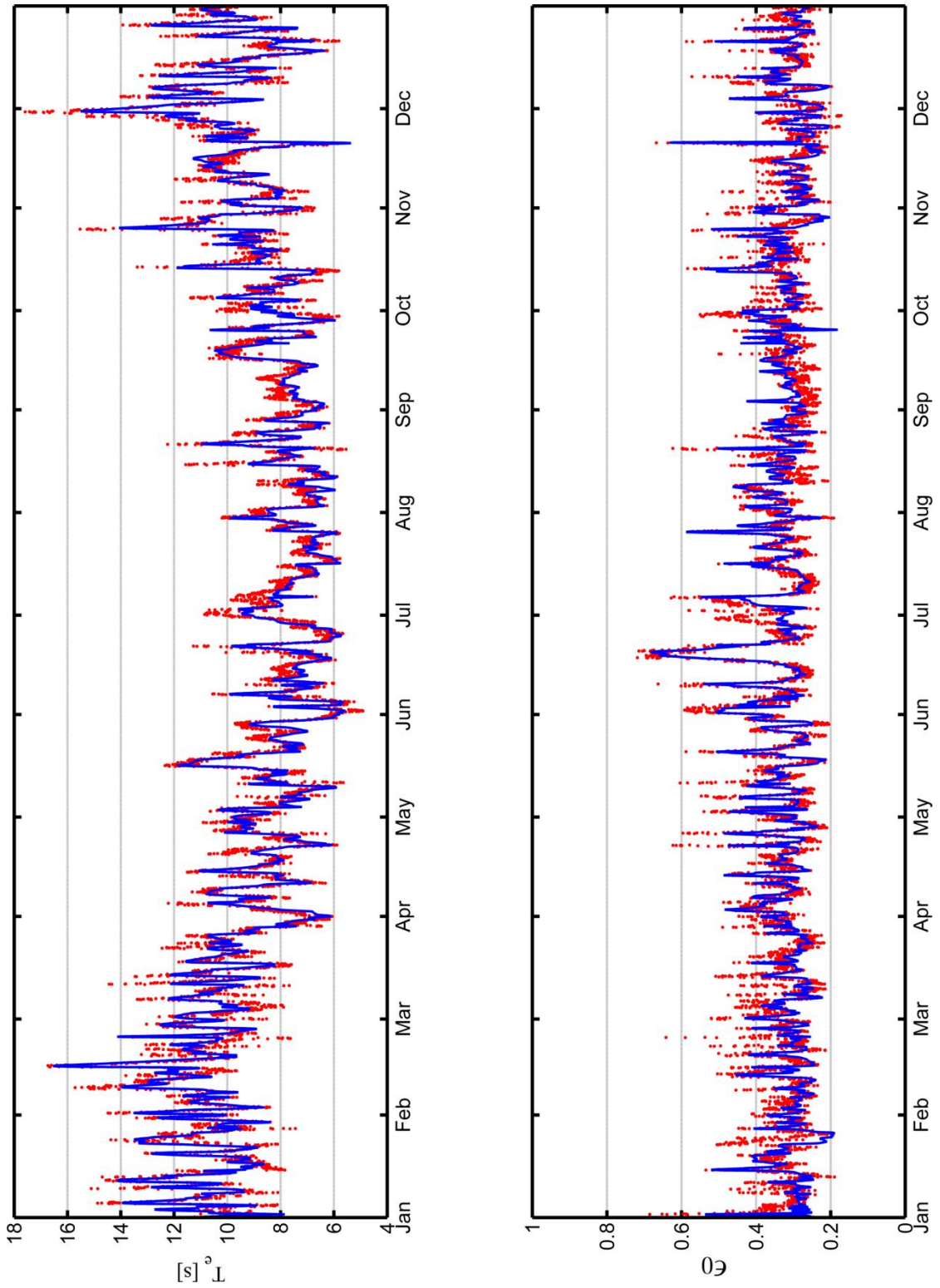
18
16
14
12
10
8
6
4
T_c [s]
Jan
Feb
Mar
Apr
May
Jun
Jul
Aug
Sep
Oct
Nov
Dec
1
0.8
0.6
0.4
0.2
0
ε0
Jan
Feb
Mar
Apr
May
Jun
Jul
Aug
Sep
Oct
Nov
Dec

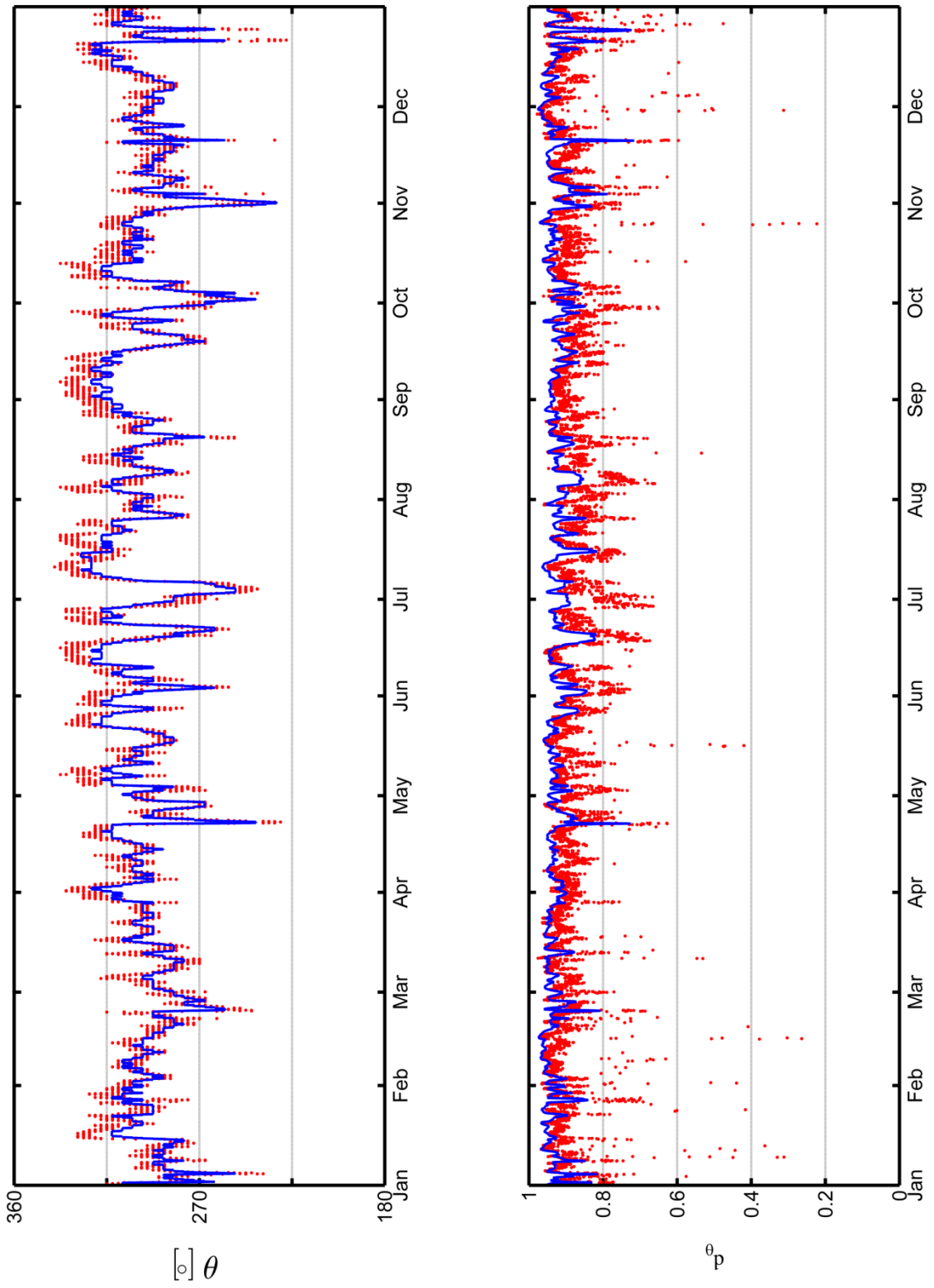

Figure 11. Comparison of IEC TS parameters calculated from the SWAN hindcast and NDBC46212 measured data are shown for the year 2008.

Table 10. Performance metrics from the García-Medina et al. (2014) hindcast.

	RMSE	PE	SI	Bias	R
OWP	22 kW/m	57%	0.64	5 kW/m	0.89
H_s	0.50 m	20%	0.21	0.03 m	0.92
T_e	1.2 s	17%	0.14	0.7 s	0.86
ν	0.10	19%	0.22	−0.03	0.23
DCO	0.15	24%	0.20	0.12	0.52
ϕ	23.9°	9%	0.09	−4.3°	0.68

DISTRIBUTION

1	MS1124	A. Dallman	6122
1	MS1124	V. Neary	6122
1	MS0899	Technical Library	9536 (electronic copy)


Sandia National Laboratories